Simulation of Arc-free Commutation of Contact with Three-material Joint in Hybrid DC Switch

[1]Chomrong Ou, [1]Nozomi Takeuchi and [1]Koichi Yasuoka

[1]Department of Electrical and Electronic Engineering, Faculty of Engineering,
Tokyo Institute of Technology, Japan

Abstract—**A hybrid DC switch (HDCS) is an effective current-interrupting device that interrupts a direct current in DC systems. A HDCS exhibits a low on-state loss and rapid current interruption. The HDCS can interrupt a low current without an arc discharge and a micro-arc for a high current interruption. However, the micro-arc still erodes the contact surface and decreases the dielectric strength between contacts, which potentially causes an arc re-ignition. In previous research, a joint copper and carbon contact was able to interrupt a 700 A current without an arc discharge by applying an increase in the contact resistance technique from copper to the carbon material of the contact. However, an arc discharge occurred when the contact changed from copper to carbon at 800 A. In this paper, the possibility of extending an arc-free interrupting current by applying a contact with copper, copper-carbon alloy, and carbon in an HDCS is presented. The contact movement and temperature are also discussed. As the simulation results show, the contact with a three-material joint can eliminate the pulse voltage, which indicates that the arc-free commutation current can be extended.**

Keywords– Hybrid DC switch, simulation, Contact resistance, arc-free commutation

I. INTRODUCTION

Direct current (DC) systems have been studied owing to their reliability and economics [1][2]. However, a DC interruption is difficult to deal with owing to the absence of a natural zero-current. An arc discharge, which ignites between the contact during a current interruption, erodes not only the contact surface, but also decreases the dielectric strength, which potentially causes an arc reignition [3]. Therefore, most studies on electric contact focuses on the elimination or mitigation of an arc discharge. The hybrid DC switch or circuit breaker has an advantage over mechanical switches and semiconductor switches for an arc-free interruption. The hybrid DC switch uses the current commutation technique to transfer the circuit current from the mechanical contact opening to the semiconductor in an on-state, and the current is interrupted by the semiconductor in an off-state [3]. In simulation of a solid-state breaker, the HDCS and a mechanical switch, it found that they had disadvantage and advantages which depends on requirement of applications. However, the simulation did not include arc discharge factor which gave advantage to the HDCS and solid-state switch [4]. ABB proposed a hybrid HVDC breaker (HVDCB) that can interrupt the current for a high DC voltage of 10 kA and 320 kV for arc-free commutation [5]. However, the on-state loss is higher because the current flows through a series of IGBTs, which have a high on-state loss; in addition, the production cost is also high owing to the number of series connections of the semiconductor device holding large current. Another hybrid DC switch with a copper and carbon contact can interrupt the current up to 700 A with arc-free commutation and a loss of on-state loss [6]. The structure of the hybrid DC switch is simple, comprising a pair of contacts, a semiconductor (SiC-MOSFET), and a number of varistors. The contact was joined with copper and carbon materials. An arc-free commutation was achieved using an increasing contact resistance technique from copper to carbon. However, an arc discharge occurred when the current increased to 800 A owing to the large difference in resistivity between the copper and carbon materials. In this paper, the possibility of increasing the arc-free commutation

current by inserting a copper-carbon alloy between the copper and carbon materials is presented. This study is carried out using a simulation.

II. MODEL AND SIMULATION

The simulation was carried out using the COMSOL Multiphysics program with a combination of four modules: heat transfer, electric current, electric circuit, and solid mechanics modules. The model was in three-dimensional (3D), and the configuration and dimensions of the contacts are as shown in Fig. 1. There were two pairs of contacts used in this study. Fig. 1(a) shows the first contact pair (the left and right contacts). The contacts were 15, 12, and 5 mm in height, width, and thickness, respectively. The left contact was made from a copper cuboid (Cu), with a carbon (C) plate joint inserted on top of the cuboid. The thickness of the carbon plate was 1 mm. The right contact was made of copper. The upper side of the right contact has a hole with a diameter of 3 mm serving as a rigid connection. The second contact pair had the same height, width, and thickness as the first contact pair. The left contact has a joint of copper, copper-carbon alloy, and carbon (Cu-C-A), as shown in Fig. 1(b). The right contact was made of copper. The properties of the three materials are listed in Table 1.
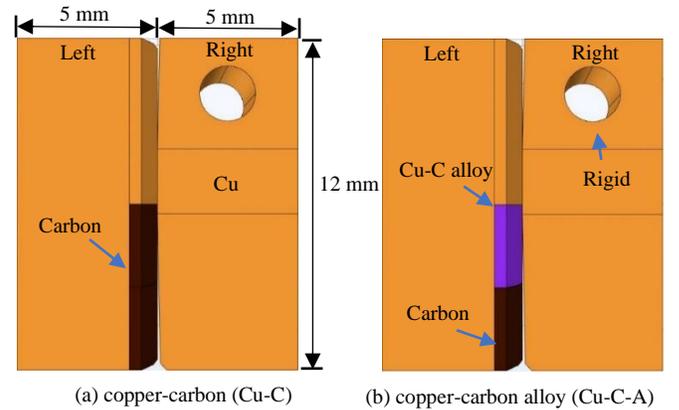

(a) copper-carbon (Cu-C)   (b) copper-carbon alloy (Cu-C-A)

Fig. 1. Two contacts with different materials used in simulation.

Table 1: Properties of Cu, Cu-C, and C materials.

Materials	Copper (Cu)	Copper-Carbon (Cu-C)	Carbon (C)
Heat capacity (J/kg. K)	385	132	132
Density (kg/m^3)	8960	1780	1780
Thermal conductivity (W/m. K)	400	175	175
Conductivity (Ω. m)	6×10^7	2×10^6	3×10^5
Resistivity temp. coeff. (1/K)	0.0039	0.005	-0.005
Reference temp. (K)	298	298	298

In the simulation, the current was fed to the contact from the voltage source V_s through a series resistor R_{cir}. The resistor R_{SiC} in series with inductor L_{stray} is connected in parallel with the contacts. Fig. 2 shows an electrical circuit diagram applied to the model. The current was 700–1000 A. The value of R_{SiC} is 4 mΩ, which represents the resistance of the SiC-MOSFET device when the SiC-MOSFET is turned on. The value of L_{stray}, which represents stray inductance of the loop circuit between the contacts and the SiC-MOSFET, is 0.1 µH. The left contact is connected to the positive terminal, and the right contact is connected to the ground.
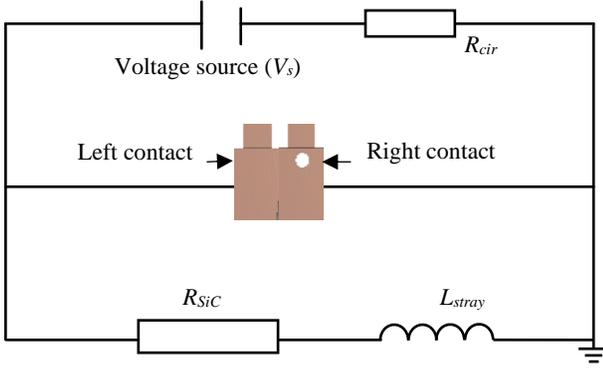

Fig. 2. Electrical circuit diagram of contact model connection.

During the opening contact process, the Solid Mechanical Module was used to move the contacts. The left contact moved to the left with an average speed of 200 m/s. The rigidity of the right contact, as shown in Fig. 1(a), is set to have a rotating spring with a spring contact of 100 N·m/rad. The right contact was pre-rotated by 15 rad in a counterclockwise direction. When the left contact moved leftward and the right contact rotated in a clockwise direction, they connected for certain length. During movement of the contact, the current flows between the contact and generates heat under Joule heating. Therefore, a heat transfer module was used to simulate the temperature in the contacts. The heat transfer module simulates the heating coupling in the electric contacts with the contact area between the contacts. The heating transfer module can specify the convective flow of air with the length of contact in the atmosphere. For calculation of coupling temperature, the electric current and Heat Transfer governing equations are involved, which indicated below,

$$\rho C_p u \cdot \nabla T = \nabla \cdot (k \nabla T) + Q \tag{1}$$

where ρ and C_p are the density and heat capacity of the material at a constant pressure, u is the velocity calculated by the solid mechanics module, T is the temperature, and Q is the heat source, coupled with the electrical module.

The Q is from Joule Heating effect which can be calculated as

$$Q = J \cdot E \tag{2}$$

where J is the current density, E is the electric field.

The current density is calculated by

$$J = \sigma E \tag{3}$$

The electric field can be calculated by

$$E = -\nabla V \tag{4}$$

where and V is the potential, and σ is the resistivity of contact material.

Fig. 3 shows the mesh along the contact contours. The actual contact area was much smaller than the entire front surface of the contact because the left and right contacts do not have perfectly flat shapes. Therefore, the contact was assigned to have a small contact area for the initial contact closing and opening. Fig. 4 shows the side and top views of the contacts. From Fig. 4(a), the right contact has a curvature (r = 100 m shape) on the top and lower parts of the contact, and a flat shape at the middle with a length of 2.35 mm along the z-axis. The contact area at the closing opposition is flat. From Fig. 4(b), the left contact has a curvature (r = 50 mm) and a flat shape for the right contact along the y-axis.
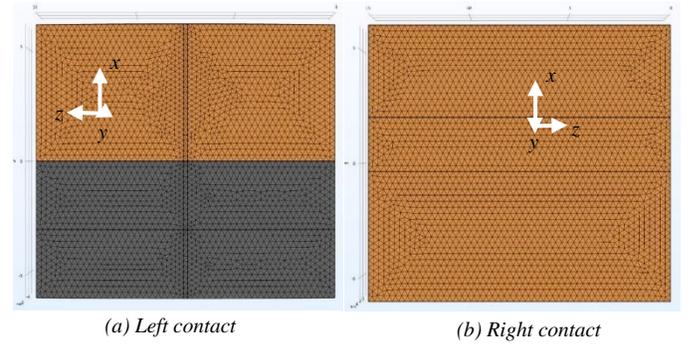

(a) Left contact   *(b) Right contact*

Fig. 3. Mesh along the contact surface in front view.
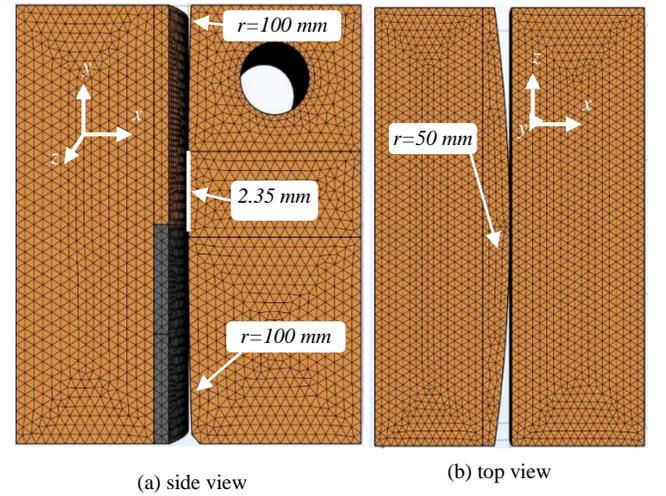

(a) side view   (b) top view

Fig. 4. Mesh and curvature along the contact surface in front view.

III. RESULTS AND DISCUSSION

3.1 Movement of contact

Fig. 5 shows the contact area of the Cu-C contacts when the contacts are in the closing position. The left contact had a joint of copper and carbon materials. The carbon material is indicated by the yellow rectangle, and the right contact is made from copper. When the contact is initially in a close position, the contact force is zero. The contact area is initially located between the copper material of both contacts, as indicated by the red rectangle in Fig. 5(b). The contact area was set to 3 mm². Fig. 6 shows the contact movement and pressure (present contact area) over time. The pressure is zero at time $t = 0$ ms. When the contact area moves at $t = 2.5$ mm, the contact pressure is located at the copper and carbon material of the left contact. The contact area was

located in the pressured area, and was smaller than this area. The contact area moves downward when the contact moves at $t = 6.28$ ms with a maximum pressure of 444 N/mm². Note that at $t = 6.28$ ms, the copper material of the left contact ruptured. The contact area continuously moves down to the carbon material of the left contact at $t = 9$ ms. The left and right contacts rupture from each other as the pressure decreases to 0 N/mm². The contact area at the copper material becomes smaller until it detaches at 6.28 ms. The carbon material detaches at 12 ms. In the overall view, the contact area moves downward from the copper to the carbon material of the left contact until the carbon material detaches with the right contact. With this movement, the contact area of the copper tends to decrease, and the contact area of the carbon tends to decrease up to time $t = 9$ ms, as shown in Fig. 6. After t = 9 ms, the contact area of the carbon starts to decrease until it reaches zero at 12 ms. This movement of the contact area increases the contact resistance over time and commutates the current to the SiC-MOSFET.
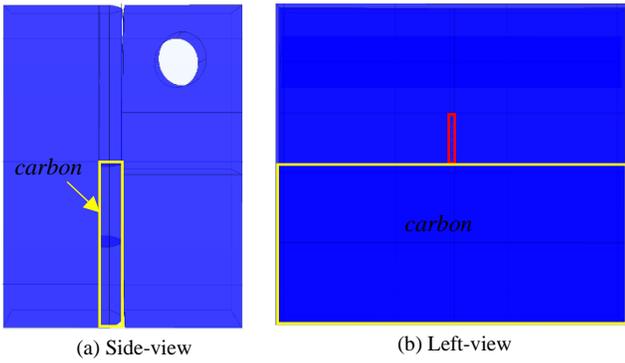

(a) Side-view   (b) Left-view

Fig. 5. Contact area Cu-C contacts in closing position.
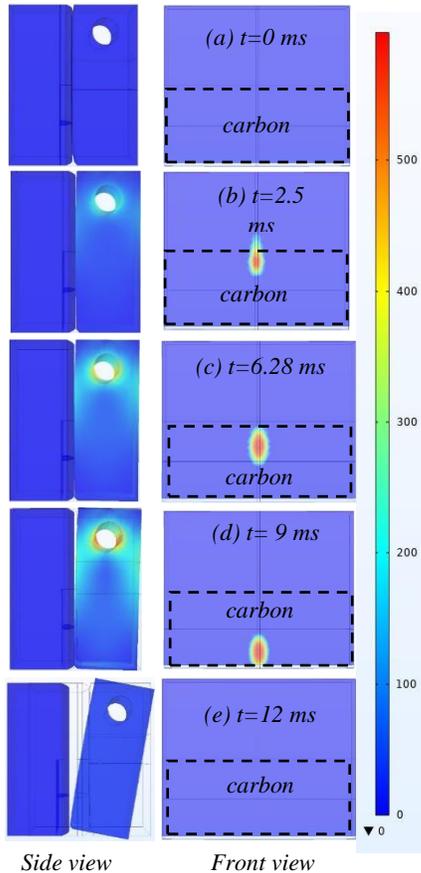

Side view   Front view

Fig. 6 Contact movement and pressure.

3.2. Contact temperature and current streamlines

The contact temperature is considered an important factor in the current commutation. When the temperature of contact exceeds the boiling temperature of the contact material as shown in Table 2 [7], the contact area ruptures, and the current cannot be commutated further. The remaining current at the contacts rapidly decreases to zero which induces a large pulse voltage causing an arc generation [8]. Fig. 7 shows the contact temperature and current streamlines during movement of the contact in a current commutation of 700 A. The

Table 2: Softening, melting, and boiling temperature of materials [7]

Material	Softening	Melting	Boling
Ag	180	960	2193
Al	150	660	2447
Au	100	1063	2817
Cu	190	1083	2582
Mo	900	2610	3700
W	1000	3380	5527

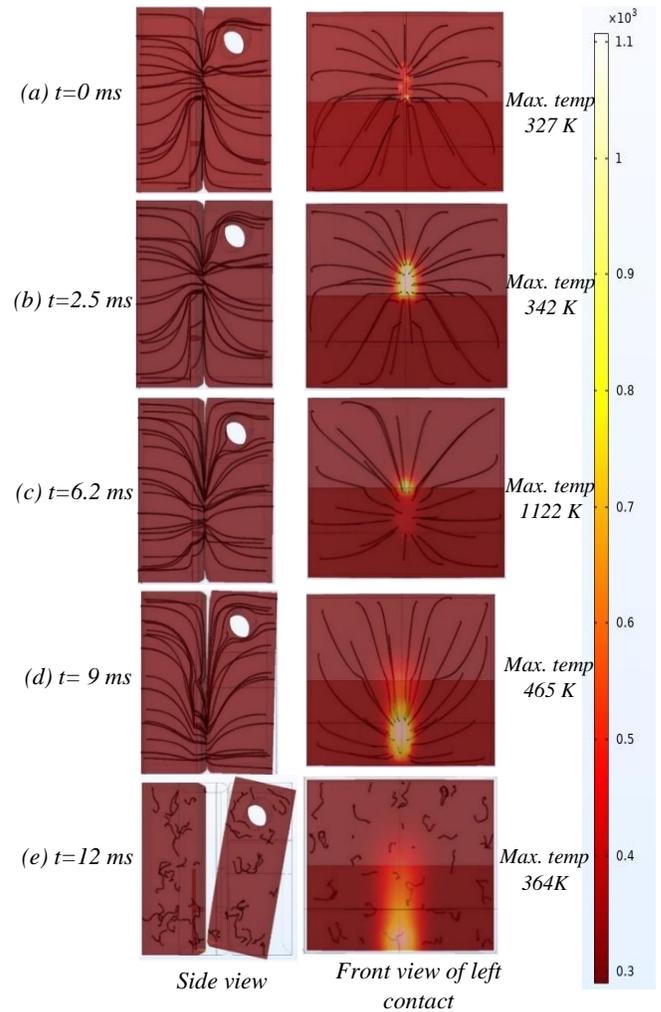Side view   Front view of left contact

Fig. 7. Temperature and current stream on the contact surfaces.

figures on the left show current streamlines through the contact area, and the right-side figures show the temperature caused by the current flow. The temperature increase follows the movement of the contact area from the initial contact area (copper) to the carbon.. For the 700 A, when the copper material of the left contact detaches at t = 6.28 ms, the temperature reaches 1122 K because of the large current flow through an extremely small area of the copper material. Although the contact area moves to the lower part of the contact area, the temperature at the previous location still increases because the current heats not only the contact area but also the vicinity of the area. When the contact area moves to the carbon material of the right contact at t = 9 ms, where the contact area is in the carbon, the temperature is 465 K because the majority of the current is commutated to the SiC-MOSFET. This means that a lower density current flows through the carbon material. When the current density decreases, the temperature also decreases as the temperature increases proportionally to the current density. When the contact detaches at t = 12 ms as both contacts rupture, the temperature decreases to 364 K, where no current flows through both contacts. Fig. 8 shows maximum temperature of Cu-C contact for 700 A (yellow line) and Cu-C-A contact for 1000 A (black line). From the start of the contact until separation for 700 A and 1000 A, the temperature did not reach the boiling temperature of the contact materials, as shown in Fig. 8. For This indicates the possibility of a larger arc-free current commutation [9].
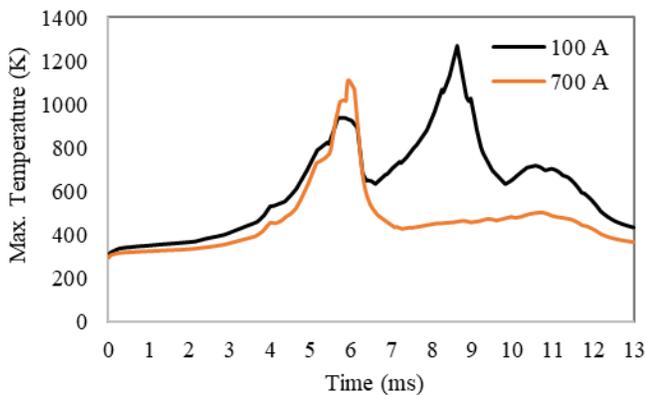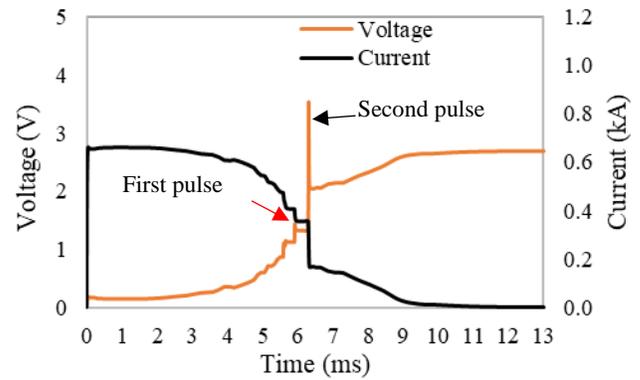
Fig. 9. Contact voltage and current waveforms of Cu-C contact for 700 A.
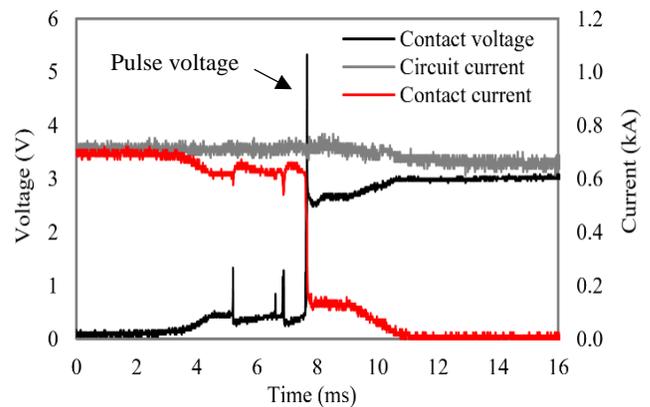
Fig. 10. Experimental waveforms of voltage and current of Cu-C contact for 700 A [6].

Fig. 8. Maximum temperature of Cu-C contact for 700 A, and Cu-C-A contact for 1000 A.

3.3 Contact current and voltage

Fig. 9 shows the contact voltage and current waveforms during the movement of the contact. At approximately 2 ms, the circuit current flowing through the contacts is 700 A, and the contact voltage is 0.14 V. From 2 ms, the left contact moves leftward and the right contact rotates clockwise to make a contact with the left contact. During the movement of the contact, the contact area moves downward, as shown in Fig. 6. The movement of the contact area increases the contact resistance because carbon has a much higher resistivity than copper. When the contact resistance increases, the contact current decreases. The decrease in contact current indicates that a partial current flows to the SiC-MOSFET (the 4-mΩ resistor shown in Fig. 2). When the contact voltage increases, the first pulse suddenly occurs at approximately 6 ms. The contact voltage then increases further until the second pulse voltage occurs at 6.28 ms. After the second pulse, the current flows through only the carbon material, and the current decreases to zero when the contacts detach from each other at t = 12 ms. No pulse occurs after the contact ruptures because the contact current decreases to almost zero before the carbon material detaches.

Fig. 10 shows the 700 A arc-free commutation for Cu-C from the experiment. Figs. 9 and 10 show the same tendency, particularly for the second pulse (during the simulation) and pulse voltage (during the experiment). The second pulse is caused by a rapid change in contact resistance when the copper material of the left contact is ruptured, and the contact resistance rapidly increases, which leads to a rapid decrease in the contact current. The rapid decrease in the contact current causes a voltage surge to occur owing to inductance in the loop circuit between the contact and SiC-MOSFET. During the experiment, the pulse voltage proceeded to an arc discharge when the circuit current was 800 A. To avoid an arc discharge, the copper-carbon alloy having a resistivity of 2×10^{-6} Ω. m) between that of copper and carbon is inserted between the copper and carbon material, as shown in Fig. 1(b), thereby preventing a large current drop at the contact and increasing the arc-free commutation current. Fig. 11 shows the contact current and voltage waveform of the Cu-C-A contact for 700 A. Unlike the Cu-C contact, there is no surge at 6.28 ms, and the current commutation does not have a large current chopping, which causes a surge voltage. Fig. 12 shows the current and voltage waveforms of Cu-C-A for 1000 A. From Fig. 12, there is no pulse during the current commutation. Without the pulse voltage during the current commutation, the arc discharge can be eliminated because the arc discharge requires a high voltage/pulse voltage to initiate. The total commutation time take about 12 ms, and it can be shorten by increasing speed of the left contact moving leftward as DC interruption requires to be quick [10].
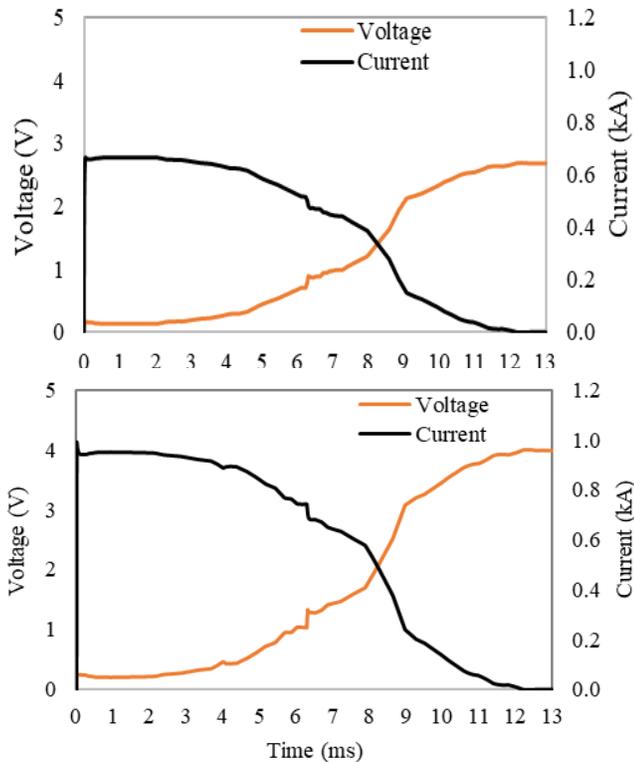
Fig. 12. Contact voltage and current of Cu-C-A contact for 1000 A.

IV CONCLUSION

The simulation was carried out using the COMSOL Multiphysics program with a combination of four modules: heat transfer, electric current, electric circuit, and solid mechanics modules. From the simulation, the contact area moved downward from the copper and carbon material of the left contact, which increased the contact resistance over time. The temperature did not exceed the melting or boiling temperature of the materials, which showed potential for increasing the current with arc-free commutation. The temperature was higher when the contact area was at the copper because of the large current through this area. The simulation results of the contact current and voltage showed a similar tendency as in the experimental results. The second surge caused by a rapid current drop can be prevented by inserting the Cu-C alloy, which has a resistivity between the copper and carbon material. The total commutation time take about 12 ms, and it can be shortened by increasing speed of the left contact moving leftward.

REFERENCES

[1] L. E. Zubieta, "Power management and optimization concept for DC microgrids," *in Proc. 2015 IEEE First Inter. Conf. on DC Micr. (ICDCM)*, PP. 81–85, June 2015.

[2] K. Yeager, "DC Microgrid performance excellence in electricity renewal," *in Proc. 2015 IEEE First Inter. Conf. on DC Micr. (ICDCM)*, pp. 377–380, June 2015.

[3] C. Ou, R. Nakayama, S. Zen, and K. Yasuoka, "Influence of a short-duration arc on the erosion and dielectric strength of narrow air-gap contacts in a hybrid DC switch," *in IEEE Trans. Compon., Packag. Manuf. Technol.*, vol. 9, no. 6, pp. 1068–1074, June 2019.

[4] M. Mobarrez, M. G. Kashani, S. Bhattacharya and R. Adapa, "Comparative study of DC circuit breakers using realtime simulations," *in Proc. IECON 40th Annual Conference of the IEEE Industrial Electronics Society*, Dallas, TX, USA, pp. 3736-3742, 2014.

[5] J. Häfner and B. Jacobson, "Proactive hybrid HVDC breakers - A key innovation for reliable HVDC grids," *CIGRE 2011 Bol. Symp. - Electr. Power Syst. Futur. Integr. Supergrids Microgrids*, 2011.

[6] C. Ou, H. Yinming, and K. Yasuoka, "New configuration of contacts for increasing the threshold current of arc-free commutation in a DC hybrid switch," *in IEEE Trans. Compon., Packag. Manuf. Technol.*, vol. 10, no. 8, pp. 1320–1327, Aug. 2020.

[7] R. Holm, "Electric Contacts: Theory and Application," 4th edit., Berlin, Germany: Springer-Verlag, 1967.

[8] P. G. Slade, "Electrical Contacts: Principles and Application," 2th edit., New York, CRC Press, Taylor & Francis Group, 2014.

[9] M. Chen, Y. Yamada, S. Zen, N. Takeuchi, and K. Yasuoka, "Study on Cu-W Clad Contact Materials with Arc-less Current Commutation in a Hybrid DC Switch," *in 2018 IEEE Holm Conference on Electrical Contacts*, pp. 166–171, 2018.

[10] S. Liu, Z. Liu, J. d. Jesus Chavez, M. Popov, "Mechanical DC circuit breaker model for real time simulations," in Transactions on International Journal of Electrical Power & Energy Systems, Vol. 107, pp 110–119, 2019.